Asian Journal of Pharmaceutical Sciences 19 (2024) 100950

Available online at www.sciencedirect.com

ScienceDirect

journal homepage: www.elsevier.com/locate/AJPS

Research Article

Hydroxyethyl starch conjugates co-assembled nanoparticles promote photodynamic therapy and antitumor immunity by inhibiting antioxidant systems

Xiang Chen[b,1], *Zhengtao Yong*[b,1], *Yuxuan Xiong*[b,1], *Hai Yang*[a,b,c,d,1], *Chen Xu*[b], *Xing Wang*[b], *Qingyuan Deng*[b], *Jiayuan Li*[b], *Xiangliang Yang*[a,b,c,d,e,f], *Zifu Li*[a,b,c,d,e,f,*]

[a] *Key Laboratory of Molecular Biophysics of Ministry of Education, Huazhong University of Science and Technology, Wuhan 430074, China*
[b] *Department of Nanomedicine and Biopharmaceuticals, College of Life Science and Technology, Huazhong University of Science and Technology, Wuhan 430074, China*
[c] *National Engineering Research Center for Nanomedicine, Huazhong University of Science and Technology, Wuhan 430074, China*
[d] *Hubei Key Laboratory of Bioinorganic Chemistry and Materia Medical, Huazhong University of Science and Technology, Wuhan 430074, China*
[e] *Hubei Engineering Research Center for Biomaterials and Medical Protective Materials, Huazhong University of Science and Technology, Wuhan 430074, China*
[f] *Hubei Bioinformatics and Molecular Imaging Key Laboratory, Huazhong University of Science and Technology, Wuhan 430074, China*

ARTICLE INFO

Article history:
Received 9 April 2024
Revised 6 June 2024
Accepted 17 June 2024
Available online 19 August 2024

Keywords:
Hydroxyethyl starch smart nanomedicine
Photodynamic therapy
Antioxidant systems
Immunogenic cell death

ABSTRACT

Photodynamic therapy (PDT) can produce high levels of reactive oxygen species (ROS) to kill tumor cells and induce antitumor immunity. However, intracellular antioxidant systems, including glutathione (GSH) system and thioredoxin (Trx) system, limit the accumulation of ROS, resulting in compromised PDT and insufficient immune stimulation. Herein, we designed a nanomedicine PtHPs co-loading photosensitizer pyropheophorbide a (PPa) and cisplatin prodrug Pt–COOH(IV) (Pt (IV)) based on hydroxyethyl starch (HES) to inhibit both GSH and Trx antioxidant systems and achieve potent PDT as well as antitumor immune responses. Specifically, HES-PPa and HES-Pt were obtained by coupling HES with PPa and Pt (IV), and assembled into nanoparticle PtHPs by emulsification method to achieve the purpose of co-delivery of PPa and Pt (IV). PtHPs improved PPa photostability while retaining PPa photodynamic properties. *In vitro* experiments showed that PtHPs reduced GSH, inhibited Trx system and had better cell-killing effect and ROS generation ability. Subcutaneous tumor models showed that PtHPs had good safety and tumor inhibition effect. Bilateral tumor models suggested that PtHPs promoted the release of damage-associated molecular patterns and the maturation of dendritic cells, induced T cell-mediated immune

* Corresponding author at: Key Laboratory of Molecular Biophysics of Ministry of Education, Huazhong University of Science and Technology, Wuhan 430074, China.
E-mail address: zifuli@hust.edu.cn (Z. Li).
[1] These authors contributed equally to this work.
Peer review under responsibility of Shenyang Pharmaceutical University.

https://doi.org/10.1016/j.ajps.2024.100950

responses, and thus suppressed the growth of both primary and distal tumors. This study reports a novel platinum-based nanomedicine and provides a new strategy for boosting PDT therapy-mediated antitumor immunity by overcoming intrinsic antioxidant systems.

1. Introduction

Photodynamic therapy (PDT) is considered as a promising cancer treatment [1]. It uses molecular oxygen to produce a large amount of reactive oxygen species (ROS), especially singlet oxygen ($^1O_2$), by photosensitizers under the excitation of a specific wavelength laser, thereby killing tumor cells and inhibiting the development and occurrence of various tumors [2–4]. Compared with other tumor treatments, PDT has the characteristics of non-invasive, space-time controllability, and low side effects [5,6]. Light, photosensitizer, and molecular oxygen are safe when administered alone, because ROS generated after illumination has a short lifetime (less than 200 ns) and a small diffusion range (about 20 nm), which limits the cytotoxicity of PDT to the illumination area [5,7]. However, photosensitizers generally have shortcomings such as poor water solubility, short blood circulation time, and lack of tumor targeting [8–10].

ROS produced by PDT cannot only induce tumor cell apoptosis but also trigger the occurrence of immunogenic cell death (ICD) [11–14]. High levels of ROS cause oxidative stress injury within tumor cells and induce calreticulin (CRT) eversion, release of high mobility group box-1 (HMGB-1), and secretion of adenosine triphosphate (ATP) [4,15,16]. These damage-associated molecular patterns (DAMPs) bind to antigen-presenting cells and activate adaptive immune responses [17–19]. However, the generation of ROS is usually limited by intracellular antioxidant systems (thioredoxin system, Trx system and glutathione system, GSH system), compromising PDT-mediated cancer cell killing and immune stimulation [20–23].

Cisplatin is a commonly used chemotherapeutic drug for Pt (II) and has been reported to be capable of suppressing thioredoxin reductase (TrxR) activity [24–26]. However, side effects of cisplatin (nephrotoxicity, ototoxicity, hepatotoxicity, gastrointestinal toxicity, etc.) and drug resistance limit the clinical application [27–29]. Tetravalent platinum prodrug Pt (IV) can overcome some shortcomings of Pt (II). Pt (IV) has a stable spatial octahedral structure and strong kinetic inertia, which alleviate side effects to some extent [30,31]. Inside the tumor cells, inactive Pt (IV) can consume GSH to be reduced to active Pt (II), helping the drug exert therapeutic effect at tumor cells selectively [32–34]. In addition, compared with Pt (II), Pt (IV) carries two additional ligands [35,36]. Therefore, Pt (IV) can be endowed with specific functions by adjusting the composition of ligands [37,38].

Hydroxyethyl starch (HES) is a widely used plasma substitute product in clinical practice [39]. It has good biosafety, low immunogenicity, excellent biodegradability, and abundant reaction sites [40]. These advantages render HES promising carrier for drug delivery. Our previous studies have demonstrated that the coupling of HES with photosensitizer can improve aqueous solubility, improve light stability, promote photosensitizer tumor targeting ability, and augment PDT efficacy [41,42]. Moreover, HES can be linked with Pt (IV) by oxidation of cisplatin to yield HES-Pt conjugates [43]. In the current study, we designed and synthesized a HES-based nano drug delivery system (NDDS), which co-delivered photosensitizer and Pt (IV) to the tumor site, promoted the generation of ROS by inhibiting intracellular antioxidant systems, and augmented PDT efficacy and antitumor immunity. Specifically, HES-PPa (HP) and HES-Pt (PtH) were prepared by conjugating HES with photosensitizer pyropheophorbide a (PPa) and HES with Pt (IV), respectively. Nanoparticles PtHPs were obtained by co-assembly of these two conjugates (HP and PtH) via an emulsification method (Scheme 1A). PtHPs improved the water solubility and photostability of photosensitizer. Compared with PPa, PtHPs had longer blood circulation time and enhanced tumor accumulation and enrichment. In addition, Pt (IV) in PtHPs could consume GSH to release Pt (II), which further inhibited TrxR activity. Therefore, PtHPs simultaneously inhibited two antioxidant systems of Trx and GSH, promoted the accumulation of ROS after laser light illumination, and achieved potent therapeutic effects and immune responses (Scheme 1B) in tumor bearing mice. This study reports a novel nanomedicine based on HES and demonstrates a new paradigm for boosting PDT and antitumor immunity by inhibiting dual antioxidant systems.

2. Materials and methods

2.1. *Materials*

HES 130/0.4 (molecular weight: 130 kDa, molar substitution of hydroxyethyl: 0.4) was donated by Wuhan HUST Life Science & Technology Co., Ltd. (Wuhan, China). PPa was purchased from Shanghai Dibo Chemicals Technology Co., Ltd. (Shanghai, China). Cisplatin, N-Ethyl-N′ -(3-dimethylaminopropyl) carbodiimide hydrochloride (EDCI, 98 %) and 4-dimethylaminopyridine (DMAP, 99 %) were bought from Aladdin Reagent Inc. (Shanghai, China). CCK-8, Annexin V-FITC/PI apoptosis detection kit, N-acetyl-l-cysteine (NAC) and calcein-AM/PI double staining kit were bought from Yeasen Biotechnology (Shanghai, China). oxidized thioredoxin reductase (TrxR) activity assay kit was purchased from Beijing Solarbio Science & Technology Co., Ltd. (Beijing, China). Enhanced ATP assay kit, GSH and GSSG assay kits were purchased from Beyotime Biotechnology (Shanghai, China).

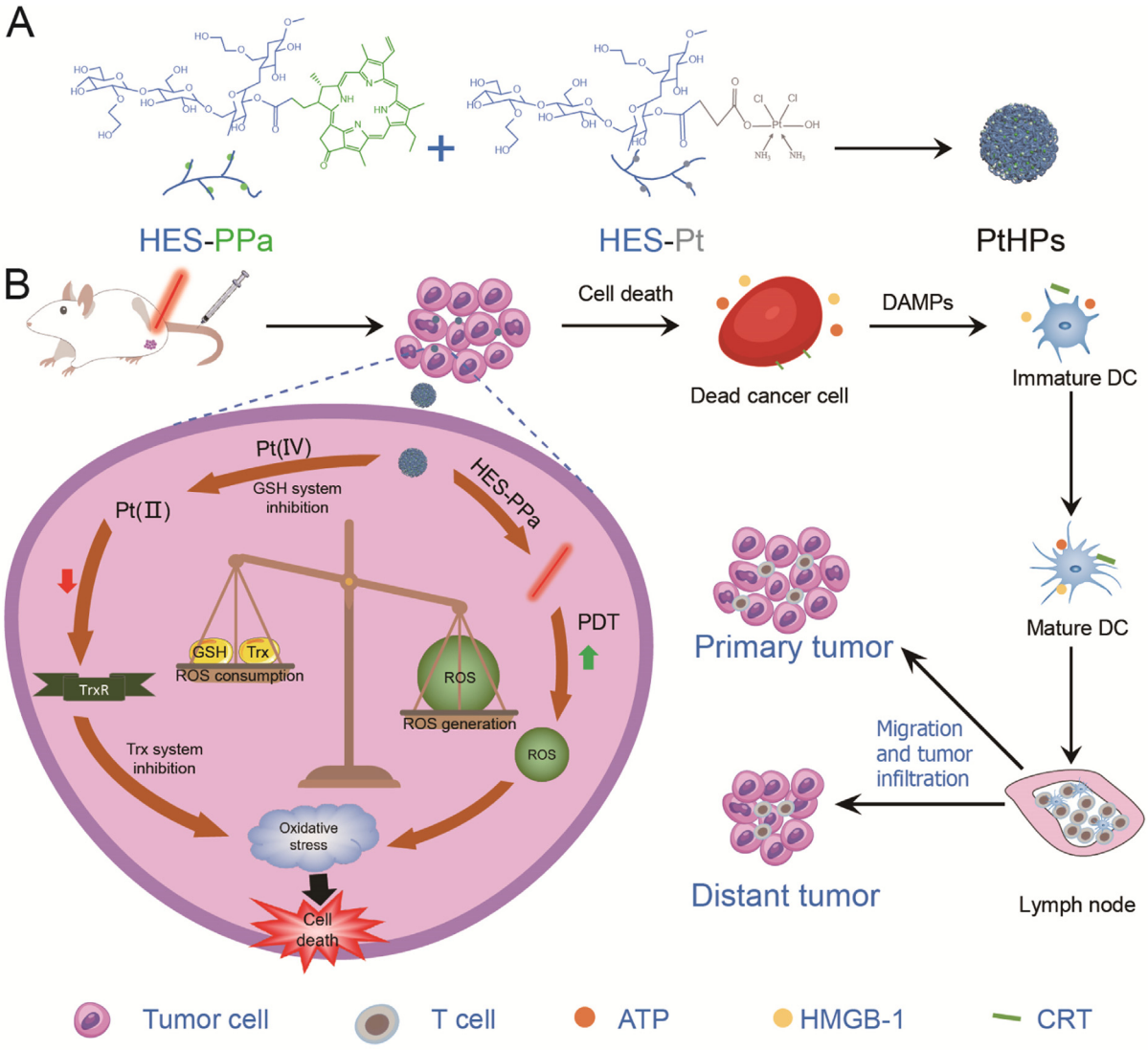

Scheme 1 – Schematic illustration of (A) nanoparticles PtHPs preparation and (B) their mechanism of inhibiting intracellular reduction systems to promote PDT and antitumor immunity in tumor-bearing mice.

DCFH-DA was bought from MedChemExpress (Shanghai, China). Mouse high-mobility protein box-1 (HMGB-1) ELISA kit was bought from Wuhan Gene Beauty Biotechnology Co., Ltd. (Wuhan, China). Flow cytometry antibodies (CD3, CD4, CD8, CD11c, CD44, CD62L, CD80, CD86, and IAIE) were bought from BioLegend (San Diego, USA).

Triple negative breast cancer (TNBC) 4T1 cell line was bought from Shanghai Institute of Biological Sciences. 4T1 cells were cultured in RPMI 1640 medium at 37 °C and 5% CO_2. The RPMI 1640 medium contained 1 % antibiotics (penicillin :100 U/ml, streptomycin :100 μg/ml) and 10 % fetal bovine serum.

BALB/c mice were purchased from Liaoning Changsheng Biotechnology Co., Ltd. The mice were kept in indoor cages at 22–24 °C with a light/dark cycle of 12/12 h and a relative humidity of 55%–60%. All animal procedures were performed in strict accordance with the internationally accepted principles and guidelines for the Care and Use of Laboratory Animals of Huazhong University of Science and Technology and the experiment protocols were approved by the Institutional Animal Ethical Committee of Huazhong University of Science and Technology.

2.2. *Synthesis of HP and PtH*

PPa (0.077 mmol) was dissolved in 20 ml DMSO, EDCI (0.31 mmol) and DMAP (0.31 mmol) were added as catalysts, and HES (1.54 mmol) were added and stirred at 30 °C for 48 h. The reaction products were precipitated with isopropyl alcohol, and then washed with isopropyl alcohol for three times. The reaction system was dissolved in DMSO, dialyzed and lyophilized to obtain the product HP. PtH was synthesized according to our previous work [43]. In short, cisplatin was dissolved in hydrogen peroxide for 1 h and centrifuged to collect precipitation. The precipitate was washed with water, ethanol and ether, and vacuum dried to obtain *c,t,c*-$[PtCl_2(OH)_2(NH_3)_2]$, the oxidation product of cisplatin. The obtained *c,t,c*- $[PtCl_2(OH)_2(NH_3)_2]$ (1.5 mmol) was dispersed

in 40 ml DMSO, then succinic anhydride (1.5 mmol) was added, and the reaction was stirred at 45 °C for 12 h. The precipitate was washed with ethanol and ether, and vacuum dried to obtain c,t,c- $[PtCl_2(OH)(OOCCH_2CH_2COOH)(NH_3)_2]$. The obtained c,t,c- $[PtCl_2(OH)(OOCCH_2CH_2COOH)(NH_3)_2]$ (0.46 mmol) was dispersed in 20 ml DMSO. EDCI (1.84 mmol) and DMAP (1.84 mmol) were added as catalysts, and the reaction was stirred at room temperature for 0.5 h, and then HES (1.54 mmol) was added. The reaction was stirred at 30 °C for 48 h. The reaction products were precipitated with isopropyl alcohol, and then washed thrice with isopropyl alcohol. The reaction system was dissolved in DMSO, dialyzed and lyophilized to obtain the product PtH. The structure was confirmed by ^{1}H NMR and FTIR. The valence change of Pt was detected by XPS.

2.3. Preparation and characterization of PtHPs

HP and PtH were dissolved in 2 ml water (mass ratio PPa:Pt = 1:2). 200 µl DCM was added to the solution, and emulsified by cell ultrasonic crusher (150 W, 2 min, 2 s/2 s). After emulsification, DCM was removed by rotary evaporation (37 °C, 4 min) to obtain PtHPs.

The particle size and zeta potential of PtHPs were detected by dynamic light scattering (DLS). The morphology of nanoparticles was observed by transmission electron microscopy (TEM), and the element distribution was confirmed by field emission TEM (FTEM). The 7-d stability of PtHPs was measured by DLS. During the experiment, PtHPs was stored in a refrigerator at 4 °C and the EP tube was shaken with the hand before determination. The spectroscopic properties of PtHPs were detected by ultraviolet spectrophotometer and fluorescence spectrometer.

The release of PtHPs: The PtHPs solution was placed in a dialysis bag (MWCO: 10 kDa), which was placed on PBS (pH 7.4, 0.1 M, 0.5% Tween-80) and shaken in a shaker with or without 10 mM GSH (37 °C, 180 rpm). 1 ml sample was taken at 5, 10, 30, 60, 120, 240, 480, 720 and 1,440 min, respectively, and the same volume of release fluid was added. The obtained samples were centrifuged (15,000 rpm, 15 min) and determined by HPLC for cisplatin concentration. The mobile phase was 0.9% NaCl solution (0.9% sodium heptane sulfonate), and the detection wavelength was 220 nm.

2.4. Photostability of PtHPs

The light stability of PtHPs was investigated by UV–vis. PPa, HP, and PtHPs (2 µg/ml of PPa) were added to a 48-well plate and irradiated with a 660 nm laser at 100 mW/cm^2. The absorbance values at 668 nm were detected at 0, 5, 10, 20, 30, 60, 90, 120, 150 and 180 s, respectively.

2.5. In vitro ROS generation

1,3-diphenylisobenzofuran (DPBF) was dissolved in ethanol to obtain DPBF stock solution (1 mg/ml). Then 25 µl DPBF solution was added to 1 ml PPa, HP, and PtHPs solution (1 µg/ml of PPa), and 1 ml corresponding solution was added to 48-well plate. The mixture was then irradiated with a 660 nm laser at 200 mW/cm^2, detecting absorbance at 405 nm every 5 s. The time attenuation of the absorbance of DPBF at 405 nm represents the ROS generation capacity. The singlet oxygen production capacity of PtHPs was further tested by electron spin resonance (ESR).

2.6. Cellular uptake

The uptake of nanoparticles by tumor cells was qualitatively studied by confocal laser scanning microscopy (CLSM, Olympus, FV3000). 4T1 cells were diluted with 1640 medium and spread into confocal dishes, with 150,000 cells in each dish, and cultured in the incubator for 12 h. HP and PtHPs were added respectively. After incubation for 12 h, the original medium was removed. Then the cells were fixed with paraformaldehyde, and DAPI was added for staining. After 15 min, the DAPI was removed and washed with PBS. After washing three times, the fluorescence of PPa in 4T1 cells was detected by CLSM.

Cultured 4T1 cells were diluted using 1640 whole medium and spread into 6-well plates, with 200,000 cells in each well, and cultured in the incubator for 12 h. HP and PtHPs were added respectively. After incubation for 12 h, the original medium was removed and washed with PBS. After washing three times, the cells were digested and collected. The fluorescence intensity of PPa was detected by flow cytometry, and the fluorescence channel was PC5.5. According to the same experimental method, the cells at 0, 1, 2, 4, 6, 8, 12 and 24 h after administration were collected respectively, and the uptake of cells over time was detected by flow cytometry.

2.7. In vitro cytotoxicity assessment

For free drug, the 96-well plates were laid with 5000 cells in each well and cultured in the incubator for 12 h. Culture medium containing PPa, cisplatin, PtH, HP, PtHPs in different concentrations was incubated for 24 h, and blank control and cell-free control groups were set up. After incubation for 24 h, a 660 nm laser was used for laser irradiation with a power of 0.2 J/cm^2. After irradiation, the 96-well plates were incubated in the incubator for 24 h. In addition, the cytotoxicity of PtHPs(+) with or without N-acetyl cysteine (NAC, 6 mM) was compared to demonstrate that ROS were responsible for killing cells. After incubation, the original medium was removed, and the cell viability was measured with CCK8 kit. Calculation of combination index (CI): $CI_{PtHPs(+)} = IC50_{PtHPs(+)}/IC50_{PtH} + IC50_{PtHPs(+)}/IC50_{HP(+)}$. $CI < 1$ indicates synergistic action, $CI > 1$ indicates antagonistic action, and $CI = 1$ indicates additive action.

2.8. Apoptosis study

4T1 cells were diluted with 1640 medium and spread into confocal dishes, with 1.5×10^5 cells in each dish, and cultured in the incubator for 12 h. PtH, HP and PtHPs were added respectively. After incubation for 24 h, a 660 nm laser was used for laser irradiation with a power of 2 J/cm^2. After irradiation, the confocal dishes were incubated in the incubator for 24 h. Staining was performed according to the instructions of the calcein-AM/PI cell activity and cytotoxicity detection kit, and photos were taken by CLSM after staining.

4T1 cells were diluted with 1640 medium and spread into 6-well plates, with 2×10^5 cells in each hole, and cultured in the incubator for 12 h. PtH, HP, and PtHPs were added respectively. After incubation for 24 h, a 660 nm laser was used for laser irradiation with a power of 2 J/cm^2. After irradiation, the 6-well plates were incubated in the incubator for 24 h. Staining according to Annexin V-FITC/PI apoptosis detection kit instructions. After staining, the apoptosis level was detected by flow cytometry.

2.9. *TrxR enzyme activity detection*

Cultured 4T1 cells were diluted with 1640 whole medium, spread into 6-well plates with 5×10^5 cells per well, and cultured in the incubator for 12 h. After cell adhesion, PtH, HP and PtHPs were added and cultured in an incubator for 24 h. The enzyme activity of TrxR was detected according to the instructions of the thioredoxin reductase (TrxR) activity detection kit. 4T1 cells were dissolved with cell lysis buffer supplemented with protease inhibitors. Centrifuge at 12,000 rpm at 4 °C for 20 min, transfer the supernatant into 1.5 ml centrifuge tube, and heat it at 100 °C for 10 min to obtain sample.

2.10. *GSH/GSSG ratio*

Cultured 4T1 cells were diluted with 1640 whole medium, spread into 6-well plates with 5×10^5 cells per well, and cultured in the incubator for 12 h. After cell adhesion, PtH, HP, and PtHPs were added and cultured in an incubator for 24 h. Intracellular GSH/GSSG ratios were measured using GSH and GSSG test kits after treatment with different drugs.

2.11. *Intracellular ROS generation*

Intracellular ROS was detected by fluorescent probe DCFH-DA. 4T1 cells were diluted using 1640 whole medium and spread into confocal dishes, each dish was spread with 1.5×10^5 cells, and cultured in the incubator for 12 h. PtH, HP and PtHPs were added respectively. After incubation for 12 h, the original medium was removed and 1 ml 10 μmol/ml DCFH-DA medium was added for incubation. After incubation for 30 min, the medium containing DCFH-DA was removed and washed with PBS. After washing three times, the medium was incubated with PBS and irradiated by 660 nm laser (2 J/cm^2 per dish). The fluorescence of DCFH-DA in 4T1 cells was detected by CLSM.

4T1 cells were diluted using 1640 whole medium and spread into 6-well plates, with 5×10^5 cells in each hole, and cultured in the incubator for 12 h. PtH, HP, and PtHPs were added respectively. After incubation for 12 h, the original medium was removed and 1 ml 10 μmol/ml DCFH-DA medium was added for incubation. After incubation for 30 min, the medium containing DCFH-DA was removed and washed with PBS. After washing three times, the medium was incubated with PBS and irradiated by 660 nm laser (2 J/cm^2). The average fluorescence intensity of DCFH-DA in 4T1 cells was measured by flow cytometry.

2.12. *Pharmacokinetics and biodistribution study*

BALB/c female mice were inoculated with subcutaneous tumors. After the tumor volume reached 200 mm^3, the tumor-bearing mice were randomly divided into 3 groups with 3 mice in each group. Free PPa, HP and PtHPs (3 mg/kg of PPa) were injected into the tail veins, respectively. Mice were anesthetized at 0, 1, 2, 4, 8, 12 and 24 h after administration, and fluorescence imaging was performed with a Caliper IVIS Lumina II *in vivo* imaging system. The *in vivo* biodistribution behavior of PtHPs was further studied. 24 h after administration, the mice were killed, and heart, liver, spleen, lung, kidney, and tumor were obtained. The fluorescence images of each organ and tumor were collected by Caliper IVIS Lumina II, and the fluorescence was quantitatively analyzed.

Free PPa, HP, and PtHPs (3 mg/kg for PPa) were administered to mice through the tail vein. After administration of 0.25, 0.5, 0.75, 1, 2, 4, 8, 12, 24 and 48 h, mouse blood was collected by cheek blood collection and stored in an anticoagulant EP tube. The blood was thoroughly mixed with anticoagulant and centrifuged at 3000 rpm for 10 min immediately, and the supernatant was taken. After that, the plasma was mixed with ultra-pure water, and then the mixture was centrifuged at 10,000 rpm for 10 min, and the supernatant was taken for assay.

2.13. *Inhibition of subcutaneous 4T1 tumors*

BALB/c female mice were purchased at 6 weeks of age with weight around 19 g. After one week of adaptive feeding in the laboratory animal room, the hair around the right hind limb of the mice was shaved. 4T1 cells were cultured to inoculate subcutaneous tumors. At inoculation, 4T1 cells were re-suspended into 10^7/ml cell suspension. A syringe was used to inject 100 μl cell suspension subcutaneously above the right hind limb of each mouse. Continue feeding after injection. The tumor volume was calculated as follows: $V=(L \times W^2)/2$, where V represents the tumor volume, L represents the long diameter of the tumor, and W represents the short diameter. When the tumor volume reaches 120 mm^3, it was recorded as Day 1. Tumor bearing mice were randomly divided into 6 groups with 8 mice in each group. Give different drugs to the tail veins. G1: saline, G2: cisplatin+PPa(+), G3: PtH, G4: PtHPs(-), G5: HP(+), G6: PtHPs(+) (1 mg/kg of PPa, 2 mg/kg of Pt). The drug was administered every three d for a total of two doses and the mice were illuminated with a 660 nm laser (180 J/cm^2) 12 h after each dose. During the experiment, mice weight and tumor volume were measured every other day. The mice were euthanized on Day 15, the tumors were stripped, and the excised tumors were weighed and photographed.

2.14. *Safety evaluation*

At the end of treatments, heart, liver, spleen, lung, and kidneys of mice in each group were harvested and stained with H&E for histological evaluation. At the same time, blood samples

of mice were collected for blood routine (WBC, RBC, HGB, PLT) and blood biochemistry (ALT, AST, BUN, CK, CREA) assays.

2.15. Preparation of single cell suspension of tumor tissues

The excised tumors were placed in 1.5 ml EP tube and crushed with sterile ophthalmic scissors. 1 ml digestive fluid containing collagenase IV and DNase I was added, digested for 1 h, and shaken for 30 min. After digestion, the cells were placed on a screen, a serum-containing medium was added, the cells were pressed vertically downward with the rubber tip of a sterile syringe, and the suspension was passed through a 200-mesh filter membrane. Centrifuge at 2,000 rpm at 4 °C for 5 min. Add PBS for cleaning, centrifuge at 2000 rpm for 5 min. Add PBS to re-suspend cells.

2.16. Flow cytometry analysis

Single cell suspensions of different groups of tumor tissues were stained with DCFH-DA, ANNEXIN V-FITC/PI apoptosis detection kit, CD44 and CD24 antibodies and analyzed by flow cytometry.

2.17. Antitumor effect of PtHPs in bilateral tumor model

BALB/c female mice were inoculated with subcutaneous tumor on one side first, and then inoculated on the other side when the tumors grew to 100 mm^3. The second d of inoculation on the other side was recorded as day 1. Tumor bearing mice were randomly divided into 4 groups with 6 mice in each group. Give different drugs to the tail veins. G1: saline; G2: PtH; G3: HP(+). G4: PtHPs(+) (1.5 mg/kg of PPa, 3 mg/kg of Pt). Light exposure (180 J/cm^2) was performed 12 h after administration. During the experiment, the mice's body weight and bilateral tumor volume were measured every other d. On the 15th d, the mice in each group were killed, the excised tumors were weighed and photographed, and spleen as well as lymph nodes were taken for further analysis.

2.18. Immune cell analysis

Tumor, spleen, and lymph node single cell suspensions were obtained. CD3, CD4 and CD8 antibodies were used to stain tumor and lymph node suspensions, and the proportion of each lymphocyte was detected. Spleen lymphocytes were stained with CD3, CD4, CD8, CD44, CD62L antibodies to detect T cells and memory T cells. CD11c, CD80, CD86 and IAIE staining were used to detect the maturation of dendritic cells (DCs).

2.19. ICD effect study

After obtaining tumor single cell suspension, CRT, HMGB-1 and ATP levels were detected according to the kit. Similar assay has been performed with 4T1 cancer cells.

2.20. Statistical analysis

All data are expressed as mean ± standard error of the mean (SEM). Statistical significance was calculated via unpaired two-tailed student's *t*-test. All statistical calculations were performed on GraphPad Prism 8.0, A P value < 0.05 was considered significant.

3. Results and discussion

3.1. Preparation and characterization of PtHPs

Conventional photosensitizers (such as PPa) have poor water solubility, low tumor targeting efficiency, and dismal light stability. Nanocarriers are promising to solve these issues [10]. When photosensitizers are coupled with hydrophilic polymers (*e.g.*, heparin, PEG, HA, etc.), aqueous solubility of photosensitizers could be enhanced. For instance, HP-PP NPs assembled by HP-PTX and HP-PPa improved water solubility of PPa, and achieved synergistic effects of chemotherapy and PDT with a tumor inhibition rate of 98.1% [44]. PTX-S-OA/PPa-PEG_{2k} NPs promoted PPa blood circulation time and accomplished a potent combination therapy between chemotherapy and PDT [45]. HA-PPa-Dendron also improved water solubility of PPa. At the same time, dendron-8Glu carried by HA-PPa-dendron could further prolong blood circulation time, increase tumor accumulation, and enhance antitumor efficacy. Tumor growth inhibition rate of HA-PPa-dendron was 99.2%, which was much higher than that of HA-PPa (50.6%) [46]. Therefore, modification of PPa with hydrophilic polymers is a feasible and powerful solution to augment PPa-mediated PDT.

HES is a widely used plasma substitute product in clinical settings while HES has good water solubility, long plasma half-life, and good biocompatibility and biosafety. HES can also be used as nanocarriers [47], either by directly conjugating with drugs, such as HES-Pt [43], or conjugating with hydrophobic polymers to prepare NDDS for delivery of free drugs [48]. Therefore, coupling PPa with HES can address some problems associated with PPa. Here, we prepared nanoparticle PtHPs by co-assembling HP and PtH (Scheme 1A).

HP (Fig. S1) was obtained by esterification of HES and PPa, and PtH (Fig. S2) was synthesized according to our previous scheme [43]. It was confirmed that HP and PtH were successfully synthesized by observing the appearance of the corresponding characteristic peaks in ^{1}H NMR (Figs. S3-S4) and the appearance of ester bond peaks in FTIR (Fig. S5). Fig. S6 is the XPS spectrum of platinum, and the result shows that Pt (II) in cisplatin is transformed into Pt (IV) after reaction. The standard curve was drawn by measuring absorbance values of PPa at 668 nm, and the drug loading of PPa for HP was 3.5%, with an average of 9 PPa per HES. The drug loading of Pt for PtH was 5.5% by ICP-OES, with an average of 37 Pt (IV) per HES. These results indicated PPa and Pt (IV) were successfully coupled to HES.

PtHPs were prepared by emulsification method, in which the drug loading of PPa was 1.5%, and the drug loading of Pt was 3%. After the preparation of PtHPs, particle size and zeta potential of PtHPs were measured by DLS. Figs. 1A and S7 show that the diameter of PtHPs was 177.8 ± 2.3 nm, the PDI was 0.145 ± 0.026, and the PtH and HP are obviously clustered. The zeta potential of PtHPs was 6.19 ± 0.71 mV (Fig. 1B), indicating that PtHPs have a positive charge and was

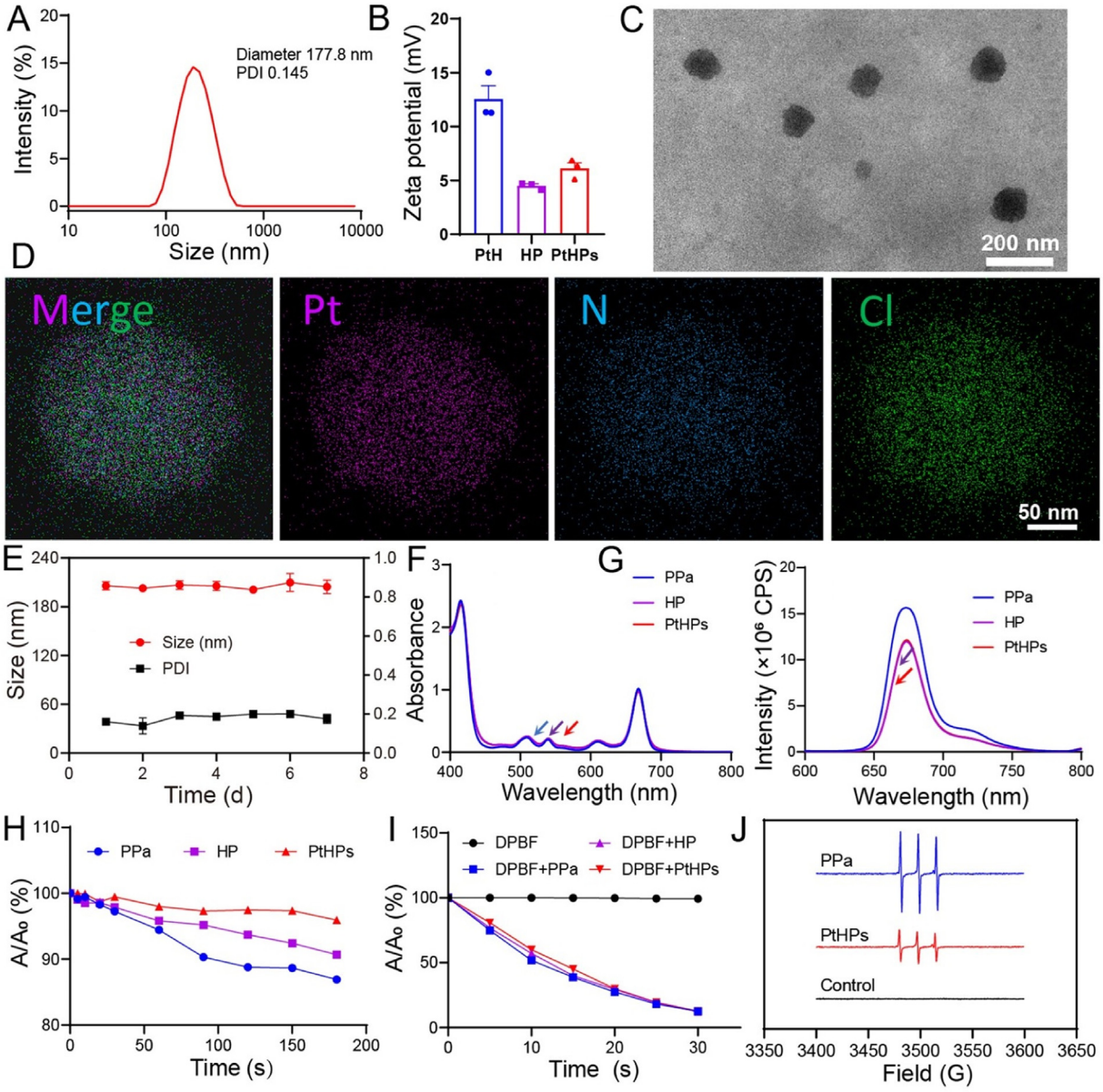

Fig. 1 – Characterization of PtHPs. (A) Hydrodynamic diameter distribution of PtHPs. (B) Zeta potential of PtH, HP, and PtHPs ($n = 3$). (C) TEM images of PtHPs; scale bar = 200 nm. (D) Elemental mapping of PtHPs; scale bar = 50 nm. (E) Colloidal stability of PtHPs in PBS for 7 d ($n = 3$). (F) UV–vis and (G) fluorescence spectra of PPa, HP and PtHPs. (H) Photostability of PPa, HP and PtHPs (2 μg/ml of PPa) in PBS under 660 nm laser irradiation (100 mW/cm^2). (I) Decay of DPBF absorbance in water/ethanol solution (water/ethanol = 40/1) at 405 nm in the presence of PPa, HP, and PtHPs (1 μg/ml for PPa) under 660 nm laser irradiation (200 mW/cm^2). (J) ESR spectra in the presence of PPa and PtHPs. Data are expressed as mean ± SEM. *P < 0.05, **P < 0.01, ***P < 0.001, ns stands for not significant.

more easily absorbed by cells. Fig. 1C showed PtHPs captured by TEM. PtHPs was spherical and the particle size was consistent with DLS data. Fig. 1D showed element mapping by FTEM. Pt, N and Cl were evenly distributed on PtHPs. The particle size distribution of PtHPs was tracked by DLS for one week. Fig. 1E and S8 show that PtHPs maintained good stability in water, PBS and FBS. The above results demonstrated that PtHPs with uniform size and good stability were prepared. Fig. 1F displayed that both HP and PtHPs had the same characteristic absorption peak as PPa. Similarly, Fig. 1G demonstrateed that both HP and PtHPs had the same fluorescence emission peak as PPa. However, the intensity was slightly different, which may be due to the ordered arrangement of PPa on HES, resulting in aggregation caused quenching (ACQ) effect in PtHPs and HP [49].

Pt (IV) consumes GSH and releases Pt (II). The release of Pt (IV) was explored here, and the results were shown in Fig. S9. In PBS solution containing 10 mM GSH (0.5% tween 80), 56.6% ± 1.3% of Pt (IV) in PtHPs was converted to cisplatin at 24 h. In the absence of GSH, Pt (IV) was barely released. This

result indicates that PtHPs have the ability to respond to GSH release.

The photostability and photodynamic effect of PtHPs were further evaluated. As shown in Fig. 1H, after irradiation of 100 mW 660 nm laser for 3 min, absorbance of PtHPs at 688 nm decreased by 4.1% ± 0.1%, and that of HP and PPa decreased by 9.3% ± 0.2% and 13.1% ± 0.1%, respectively. These results show that HES modified HP can improve photostability of PPa, while nanostructure confers PtHPs the best photostability. Subsequently, 1,3-diphenylisobenzofuran (DPBF) probe was used to detect the ability of different components to generate ROS under 660 nm laser irradiation. Fig. 1I shows that free PPa, HP, and PtHPs all could generate abundant ROS, indicating that the modification or assembly into nanoparticles has insignificant effect on photodynamic activity of PPa. Finally, using the probe 2,2,6,6-tetramethylcapsid (TEMP) as the trapping agent, typical 3 spectral lines were observed with an integral ratio of 1:1:1 (Fig. 1J), indicating that $^1O_2$ was produced [50]. Together, the above results demonstrate that PtHPs can improve photostability while retaining potent photodynamic performance of PPa.

3.2. *Cellular uptake and* in vitro *cytotoxicity*

The cellular uptake behavior of drugs is very important for drug function [51]. Firstly, the uptake of HP and PtHPs by 4T1 cancer cells was evaluated with CLSM and flow cytometry. As shown in Figs. 2A and S10, both PtHPs and HP are internalized by 4T1 cancer cells and no difference can be detected between PtHPs and HP. Furthermore, Fig. S11 illustrates that the cellular uptake of PtHPs is time-dependent.

The cytotoxicity of different formulations was determined by CCK-8. Firstly, free drugs were evaluated. Fig. S12 and Table S1 show that PPa and cisplatin display a synergistic effect on killing 4T1 cancer cells. Next, 4T1 cancer cells were incubated with different concentrations of PtH, HP, and PtHPs, and irradiated with a 660 nm laser. The results are displayed in Fig. 2B. To get a more accurate IC50 of PtH, we did a higher concentration of Pt administration (Fig S13). The half maximum inhibitory concentration (IC50) of PtH is 10.78 μg/ml. After illumination, the IC50 is 1.14 μg/ml and 0.50 μg/ml for HP and PtHPs, respectively. These results indicate that PtHPs have the best cell killing effect among all groups. Combination index (CI) is 0.5295, suggesting that there is a good synergistic effect between platinum and PDT of PtHPs. Then, Annexin V-FITC/propidium iodide (PI) kit was used to detect apoptosis. Fig. 2C and D demonstrate that PtHPs(+) could induce the highest apoptosis level (51.7% ± 0.4%), followed by HP(+) and PtH with apoptosis ratios of 47.8% ± 0.4% and 38.6% ± 0.4%, respectively. The calcein-AM/PI co-staining experiment showed the same trend (Fig. 2E).

3.3. *PtHPs promote ROS generation by inhibiting intracellular antioxidant systems*

PDT is inhibited by intracellular reduction systems. Here, Pt (IV) can consume intracellular GSH to obtain Pt (II), which can inhibit TrxR activity [26,34]. Simultaneous inhibition of GSH system and Trx system, two important intracellular reduction systems, could boost PDT. To further understand the synergistic effect between the two components of PtHPs, we detected the changes of Trx system and GSH system after treatments. Fig. 3A shows that both PtH and PtHPs significantly inhibit TrxR activity because they contain platinum, in good agreement with others [25]. In striking contrast, HP containing no platinum hardly inhibits TrxR activity. Fig. 3C shows both PtH and PtHPs significantly downregulate TrxR proteins. Fig. 3B and D corroborate that PtHPs repress TrxR expression and activity in a dose-dependent manner. The effects of different formulations on GSH system were explored as well (Fig. 3E). Similar with the Trx system, PtH and PtHPs containing Pt could significantly reduce GSH/GSSG ratio by 18.7% ± 1.6% and 21.4% ± 2.1%, respectively, whereas HP exerts little impact on GSH/GSSG ratio. To confirm the role of the reduction systems in boosting PDT, NAC replenishment experiments were performed. The cell killing effect of PtHPs(+) with or without NAC was carried out. Fig. 3F shows that the IC50 of PtHPs(+) is 0.54 μg/ml without NAC while IC50 is 0.76 μg/ml with NAC supplementation, indicating that the reduction systems have an inhibitory effect on PDT. Similar results have also been reported by others [52].

Finally, the effect of PDT was studied by exploring the production of ROS. The DCFH-DA probe was used to measure the generation of ROS after treatments with different formulations (Fig. 3G and 3H). Fig. 3G shows that PtH results in a 1.48-fold increase in intracellular ROS, presumably via simultaneously depleting GSH and inhibiting TrxR activity (Fig. 3A and 3E). HP(+) causes the ROS burst due to its photodynamic action, and ROS increases by 1.25-times relative to control. PtHPs(+) achieves the highest level of ROS, through PPa-mediated photodynamic effects (Fig. 1I) and inhibition of intracellular dual reduction systems (Fig. 3A and 3E), which is 3.05-times of control. Based on the above results, the synergistic effect between the two components of PtHPs is derived from the fact that Pt can inhibit dual antioxidant systems (GSH system and Trx system) and promote the accumulation of ROS after PDT, thereby achieving the best killing effect among all groups.

3.4. In vivo *pharmacokinetics and biodistribution evaluation*

After completing the *in vitro* study of PtHPs, *in vivo* study of PtHPs was further performed. Before performing pharmacodynamic study, the pharmacokinetics and biodistribution of different formulations were investigated. Orbital blood of BALB/c mice was collected at different time points to study pharmacokinetic behavior of different formulations, and the blood concentration-time curve of PPa was fitted with a single compartment model. As shown in Fig. 4A and Table S2, $T_{1/2}$ of HP and PtHPs were 1.46 h and 1.92 h, respectively, much higher than free PPa (0.29 h). In addition, compared with the free PPa, the $AUC_{0\sim\infty}$ of HP and PtHPs was increased by 4.80 times and 5.49 times, respectively. These results showed that PtHPs had a longer half-life and higher bioavailability than PPa. The biodistribution of different formulations in mice bearing 4T1 subcutaneous tumors was evaluated by detecting the fluorescence of PPa with an *in vivo* imaging system. As shown in Fig. 4B and 4C, free PPa could

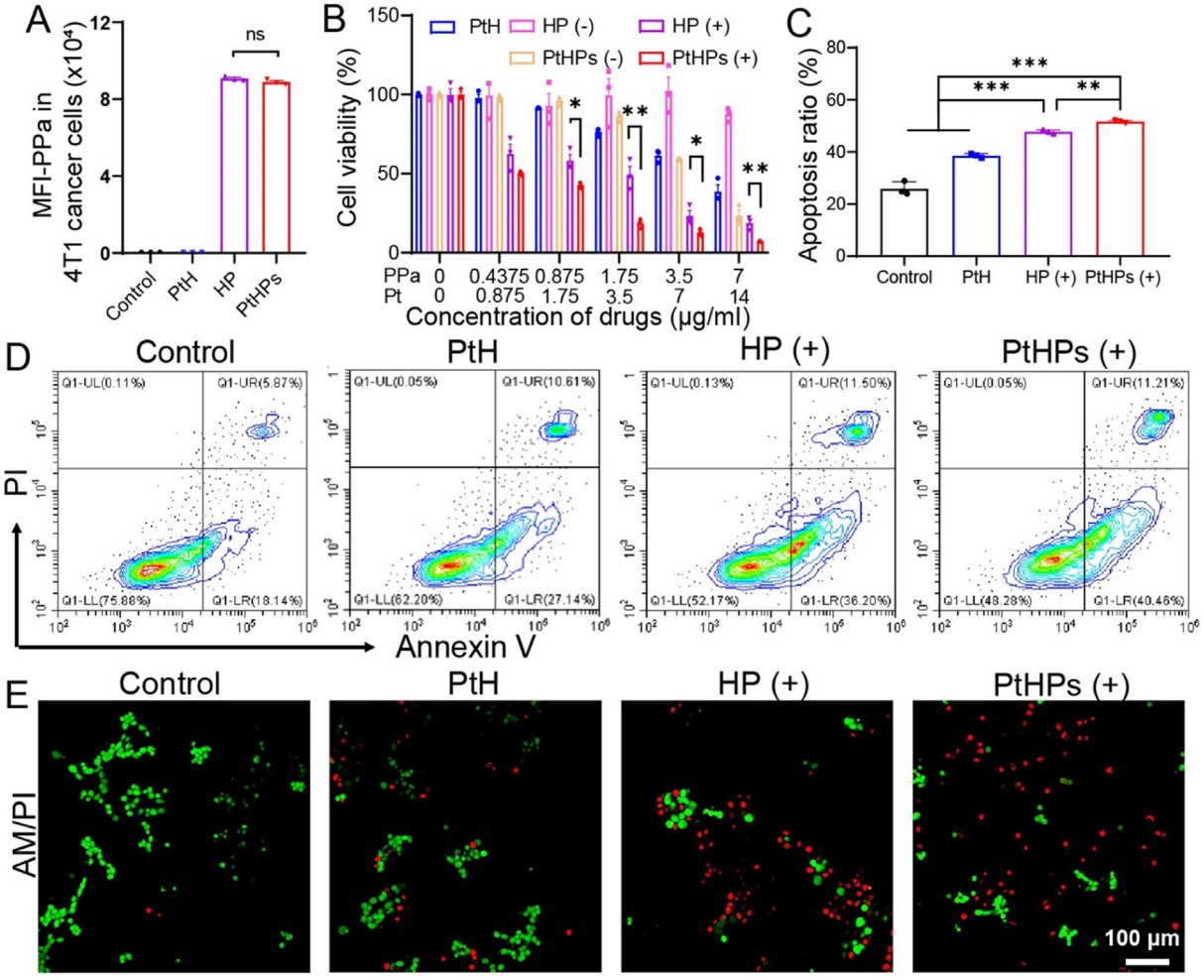

Fig. 2 – *In vitro* anticancer treatment of PtHPs. (A) Mean fluorescence intensity (MFI) of cells after treatment with PtH, HP and PtHPs by flow cytometry ($n = 3$). (B) Cytotoxicity after different treatment ($n = 3$). (C) The apoptosis percentage of 4T1 cells treatment with PtH, HP(+), and PtHPs(+) ($n = 3$). (D) The apoptosis of 4T1 cells analyzed by flow cytometry. (E) Live/dead staining images of 4T1 cells treatment with PtH, HP(+), and PtHPs(+); Scale bar: 100 μm.

hardly accumulate at tumor site; HP lacking tumor targeting could not enrich in high concentration at the tumor site. In contrast, PtHPs achieves high concentration and long-term accumulation at the tumor site. After administration for 24 h, the mice were sacrificed, the main organs and tumors were excised, and *ex vivo* imaging was performed. Fig. 4D and 4E show that no significant fluorescence of PPa is detectable at the tumor site in free PPa group. Fluorescence is observed in HP group. However, the strongest fluorescence is noticed in PtHPs-treated tumors among all groups. These results collectively indicate that PtHPs conspicuously prolong PPa blood circulation and augment PPa tumor accumulation and enrichment.

3.5. In vivo *antitumor effect of PtHPs*

Long circulation and good tumor targeting and enrichment suggest that PtHPs might have excellent antitumor effect *in vivo* [53]. To test this hypothesis, a 4T1 subcutaneous tumor model was constructed. When tumor volume reached about 120 mm^3, it was recorded as Day 0 and various formulations were administered on Day 1 and 4 (Fig. 5A). Since PtHPs achieved the highest enrichment at the tumor site at 12 h (Fig. 4C), the illumination time was selected as 12 h after administration. During the treatments, body weight and tumor volume of each mouse were recorded every two d (Fig. 5B and 5C). The mice were sacrificed on the 15th d to obtain tumors and major organs. As indicated in Fig. 5B–5F, cisplatin+PPa(+), PtH and PtHPs(-) groups displayed similar antitumor efficacy, with tumor inhibition rate (TIR) of 26.3%, 22.6% and 23.0%, respectively. Because metabolism of PPa in cisplatin+PPa(+) group was fast, there was negligible PDT effect on the tumor site during light irradiation. Antitumor efficacy of these three groups was mainly caused by Pt. Mice in the cisplatin-containing group were observed to lose significant weight during treatment, indicating significant toxicity of cisplatin (Fig. 5C). While free cisplatin exhibited evident side effects to mice, the modified Pt had negligible side effects. HP improved aqueous solubility of PPa, and could remain in the tumor site 12 h

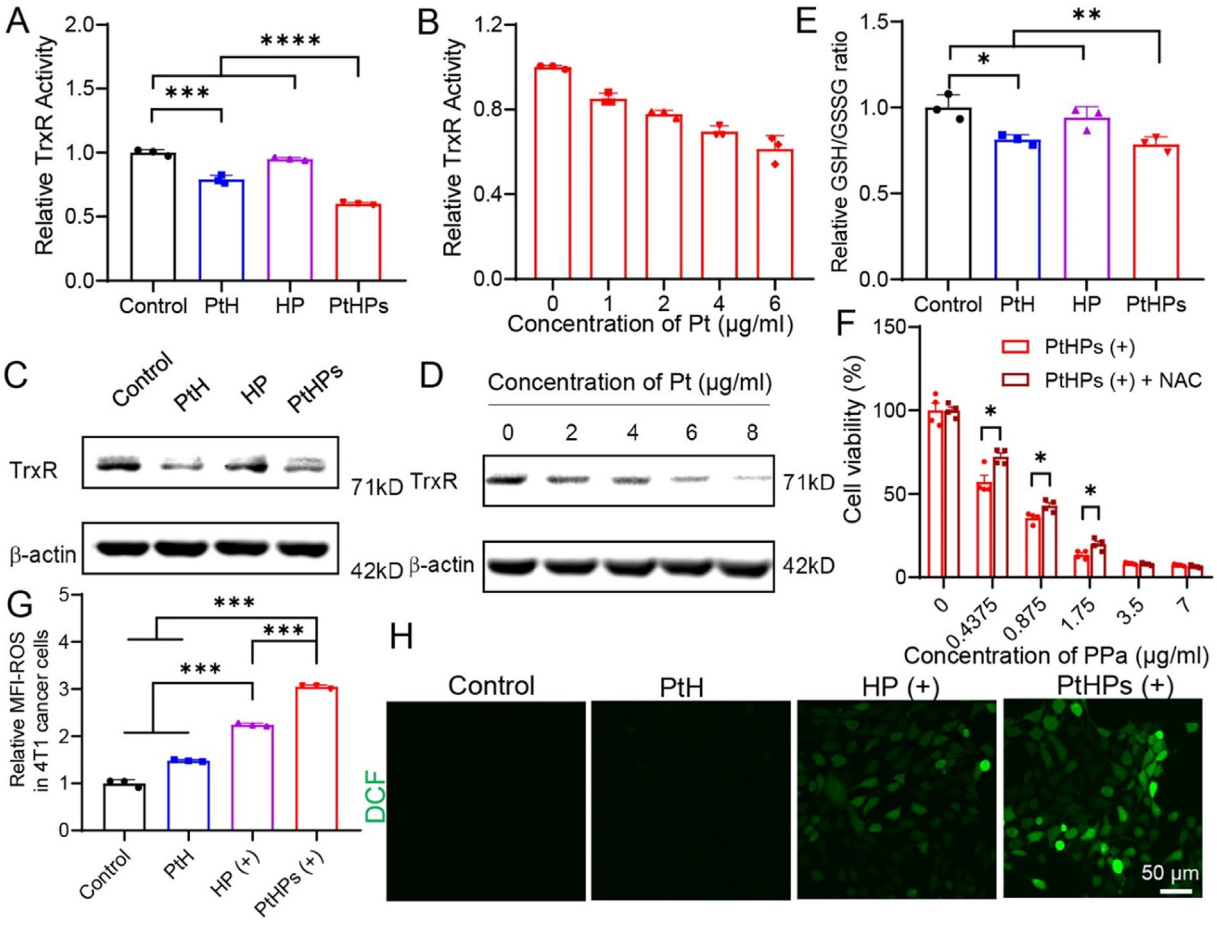

Fig. 3 – PtHPs promote ROS production by inhibiting intracellular reduction systems. (A) Enzyme activity of TrxR in 4T1 cells after different treatments ($n = 3$). (B) Enzyme activity of TrxR in 4T1 cells treated with different concentrations of PtHPs ($n = 3$). (C) Western blot analysis of TrxR protein in 4T1 cells after different treatments. (D) Western blot analysis of TrxR protein in 4T1 cells treated with different concentrations of PtHPs. (E) Relative GSH/GSSG ratio in 4T1 cells with different treatments ($n = 3$). (F) Cell viability of 4T1 cells incubated with PtHPs with or without NAC ($n = 4$). (G) Relative MFI of DCFH-DA after different treatments ($n = 3$). (H) Images of the ROS generation in 4T1 cells after different treatments; scale bar = 50 μm. Data are expressed as mean ± SEM. *P < 0.05, **P < 0.01, ***P < 0.001, ns stands for not significant.

after administration (Fig. 4C). Therefore, HP(+) achieved a better therapeutic effect after light illumination, with TIR of 49.2% ± 6.4%. PtHPs(+) has the best therapeutic effect (TIR: 77.1% ± 4.0%) among all groups, which could be ascribed to long circulation ability and good tumor targeting and enrichment capacity (Fig. 4C). Besides, PtHPs effectively inhibit intracellular reduction systems (GSH system and Trx system) through Pt to promote the accumulation of PPa-generated ROS (Fig. 3). Fig. 5G confirms that the average fluorescence intensity of ROS in PtHPs(+) is twice that of HP(+). Then, we detected apoptosis of tumor cells. As shown in Fig. 5H, there was insignificant apoptosis in the groups of cisplatin+PPa(+), PtH, and PtHPs (-), indicating that platinum alone was insufficient to evoke excessive tumor cells death. PtHPs(+) group induced 83.2% ± 1.0% apoptosis, which was significantly higher than that of HP(+) group (72.0% ± 6.2%), suggesting that the combination of PDT and Pt could indeed improve therapeutic effect. In addition, as shown in Fig. 5I, H&E staining, Ki67 staining and cleaved caspase-3 staining showed that PtHPs(+) group could lead to more necrosis, more apoptosis, and less proliferation relative to other groups. Fig. S15 shows that PDT reduces $CD44^{+}CD24^{-}$CSCs in tumors, which remains to be further explored.

The biosafety of various formulations was also evaluated. During the treatments, except for a slight decrease in body weight of mice in cisplatin group (G2), body weights of mice in other groups were relatively stable (Fig. 5C). Furthermore, no obvious lesion was observed in H&E staining of main organs (heart, liver, spleen, lung, and kidney) in all groups (Fig. S16). The blood biochemistry and blood routine of mice in each group were within normal range (Fig. S17), confirming that our nanotherapeutics are safe. Not only cisplatin, but also coupling doxorubicin with HES can significantly improve safety [48]. The above results indicate that HES based nanomedicine has good biosafety. In addition to therapeutic effects, after PtHPs(+) treatment, tumor cells displayed a higher level of CRT surface exposure while the level of T cells infiltration in tumor sites was significantly higher than that

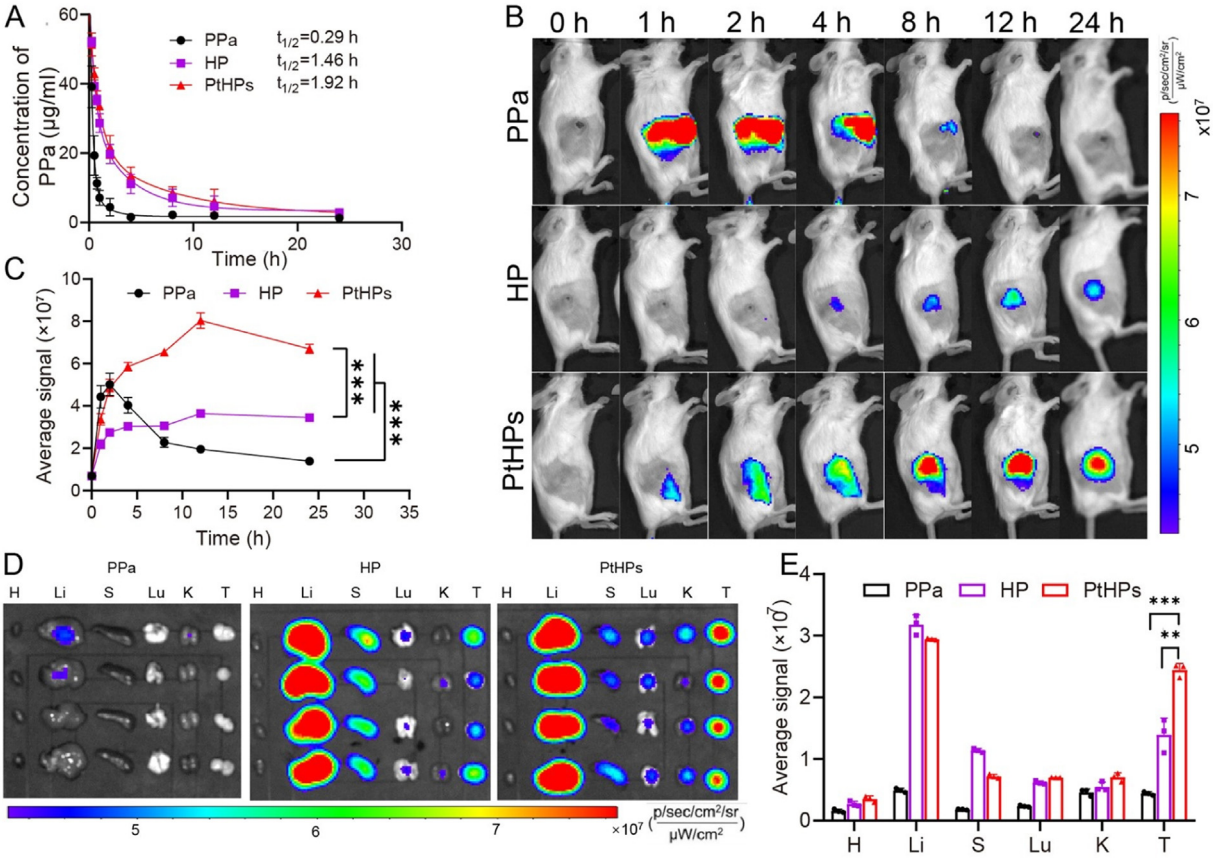

Fig. 4 – Pharmacokinetic and biodistribution of PtHPs. (A) Pharmacokinetic curves within 24 h treated with PPa, HP, or PtHPs ($n = 3$). (B) *In vivo* fluorescent images of 4T1 tumor-bearing BALB/c mice treated with PPa, HP, or PtHPs, and (C) their corresponding fluorescence intensities in the tumor areas at different points in time ($n = 3$). (D) *Ex vivo* fluorescence images of major organs and tumors isolated from mice at 24 h treated with PPa, HP, or PtHPs, and (E) their corresponding fluorescence intensities ($n = 4$). Data are expressed as mean ± SEM. *$P < 0.05$, **$P < 0.01$, ***$P < 0.001$, ns stands for not significant.

of PBS group (Fig. S18), suggesting that PtHPs have potently stimulated antitumor immune responses.

3.6. In vivo *antitumor immune responses of PtHPs*

PDT can trigger immune responses by inducing ICD, such as CRT eversion, HMGB-1 release, ATP secretion, and promote DCs maturation and T cell-mediated immune responses [54]. Validation was first performed with cellular experiments. After PtHPs(+) treatment, the CRT level exposed on the surface of 4T1 cancer cells was 2.5 times that of control group (Fig. S19). In addition, the release of HMGB-1 and secretion of ATP in PtHPs(+) were also significantly enhanced (Fig. S19). The above results indicate that HP(+) can induce ICD, while the combined treatment of PtHPs(+) can induce the strongest ICD effects among all groups.

To explore antitumor immune responses induced by PDT *in vivo*, a bilateral tumor model was constructed. As shown in Fig. 6A, primary tumor was inoculated on one side of the mouse, and distant tumor was inoculated on the other side when the primary tumor grew to around 100 mm^3. The next day after inoculation of the distant tumors, various formulations were administered and the primary tumor was illuminated. Body weight and tumor volume on both sides of each mouse were recorded every 2 d Fig. 6B shows that after bilateral tumor inoculation, there was no significant abnormality in body weight of mice, indicating that bilateral tumors did not cause serious burden on mice. The treatment results are displayed in Fig. 6C–6F. These results show that PtHPs(+) has a good therapeutic effect on primary tumors, with a TIR of 75.4% ± 5.8%; PtHPs(+) also has the best inhibitory effect on distant tumors, with a TIR of 52.7% ± 9.2%. However, administration of PtH exerts marginal effects on neither primary tumors nor distant tumors, suggesting that the excellent inhibitory effect of PtHPs(+) group on distant tumors does not originate from therapeutic effect of Pt. PDT-induced ICD effects was further explored *in vivo*. Fig. 6G–6I demonstrate that PtHPs(+) achieves the highest levels of CRT eversion, HMGB-1 release, and ATP secretion. These results are consistent with *in vitro* findings (Fig. S19). These results suggest that PtHPs(+) can induce ICD both *in vitro* and *in vivo*.

The occurrence of these phenomena indicates that PtHPs(+) potently induces ICD effects. The relationship between ICD and DC activation was further explored. The

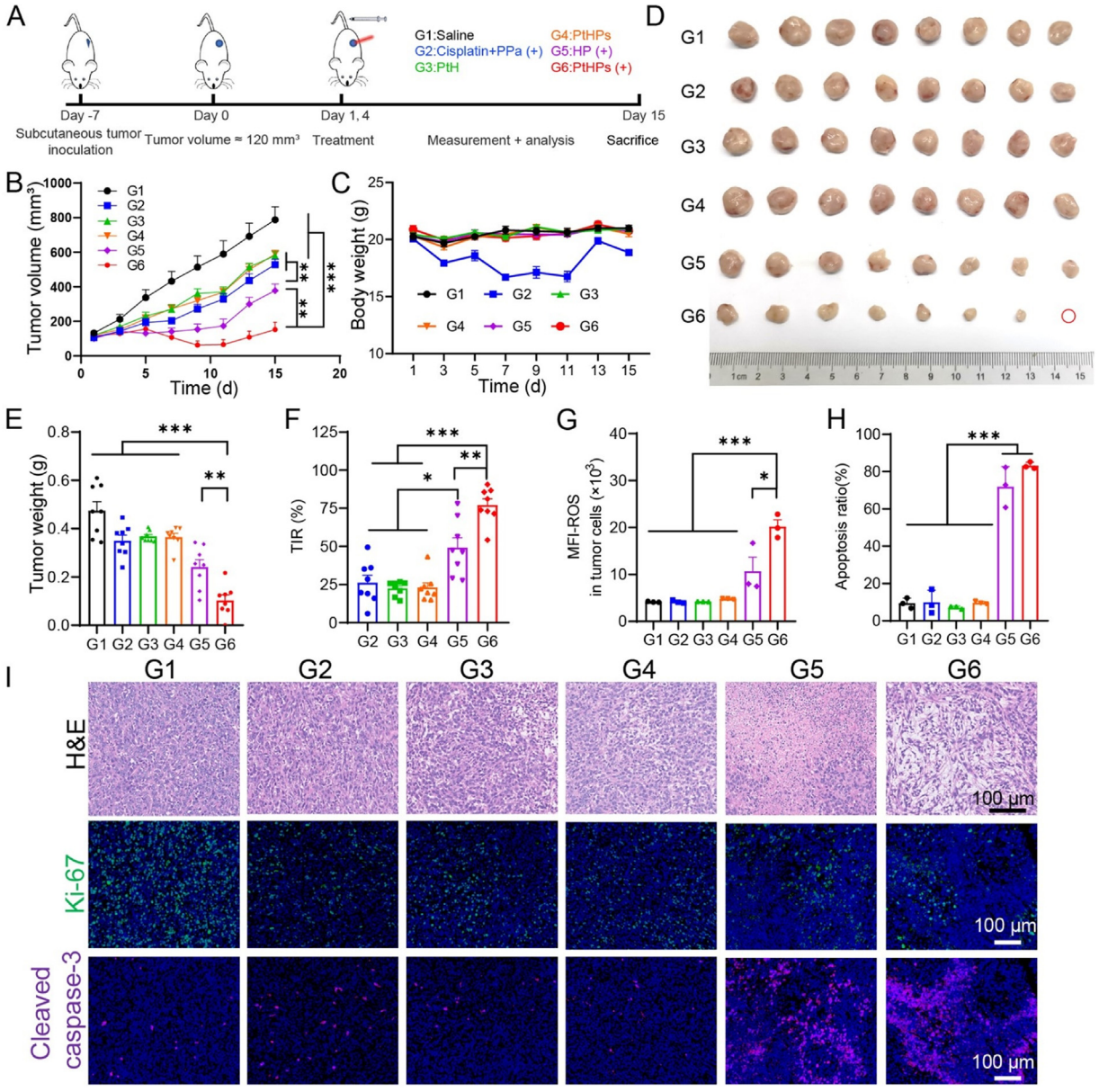

Fig. 5 – Antitumor effects of PtHPs in subcutaneous tumor model. (A) Experimental design. (B) Tumor growth profiles after treatment with different formulations ($n = 8$). (C) Body weight changes ($n = 8$). (D) Images of tumor tissues at the end of treatments. (E) Tumor weights at the end of the experiment ($n = 8$). (F) TIR in each group calculated from tumor weights ($n = 8$). (G) ROS levels in tumor tissues after different treatments ($n = 3$). (H) Quantification of apoptotic cells in tumor tissues ($n = 3$). (I) H&E, Ki-67, and cleaved caspase-3 staining images of tumor tissues at the end of treatments. G1: saline, G2: cisplatin+PPa(+), G3: PtH, G4: PtHPs(-), G5: HP(+), G6: PtHPs(+). Data are expressed as mean ± SEM. *P < 0.05, **P < 0.01, ***P < 0.001, ns stands for not significant.

maturation of DCs ($CD11c^+CD80^+CD86^+$) in tumor draining lymph nodes was detected. The results are shown in Figs. 7A and S20. After PtHPs(+) treatment, $CD11c^+CD80^+CD86^+IAIE^+$ cells increased from 51.5 % ± 2.0 % to 63.8% ± 0.7%, indicating that PtHPs(+) treatment can induce DC maturation through ICD, which is beneficial for T cell-mediated immune responses. After PtHPs(+) treatment, the proportion of tumor-infiltrating lymphocytes (CD3) in primary tumors and distant tumors also increased significantly (Fig. S21, S22), which were 1.91 times and 1.86 times that of control group, respectively. These results suggest that PtHPs(+) can promote T cell infiltration in both primary and distal tumors by inducing DC maturation. $CD8^+$ cytotoxic T lymphocytes (CTL) in tumors were further examined (Fig. 7D and 7E). After PtHPs(+) treatment, more $CD8^+$ CTL was detected in primary tumors and distant tumors, which was 2.10 times and 2.01 times of the control group, respectively. The proportion of $CD4^+$ helper lymphocytes in primary tumors and distant tumors of PtHPs(+) group was also significantly higher than that of other groups, which was 2.24 times and 2.02 times that of control

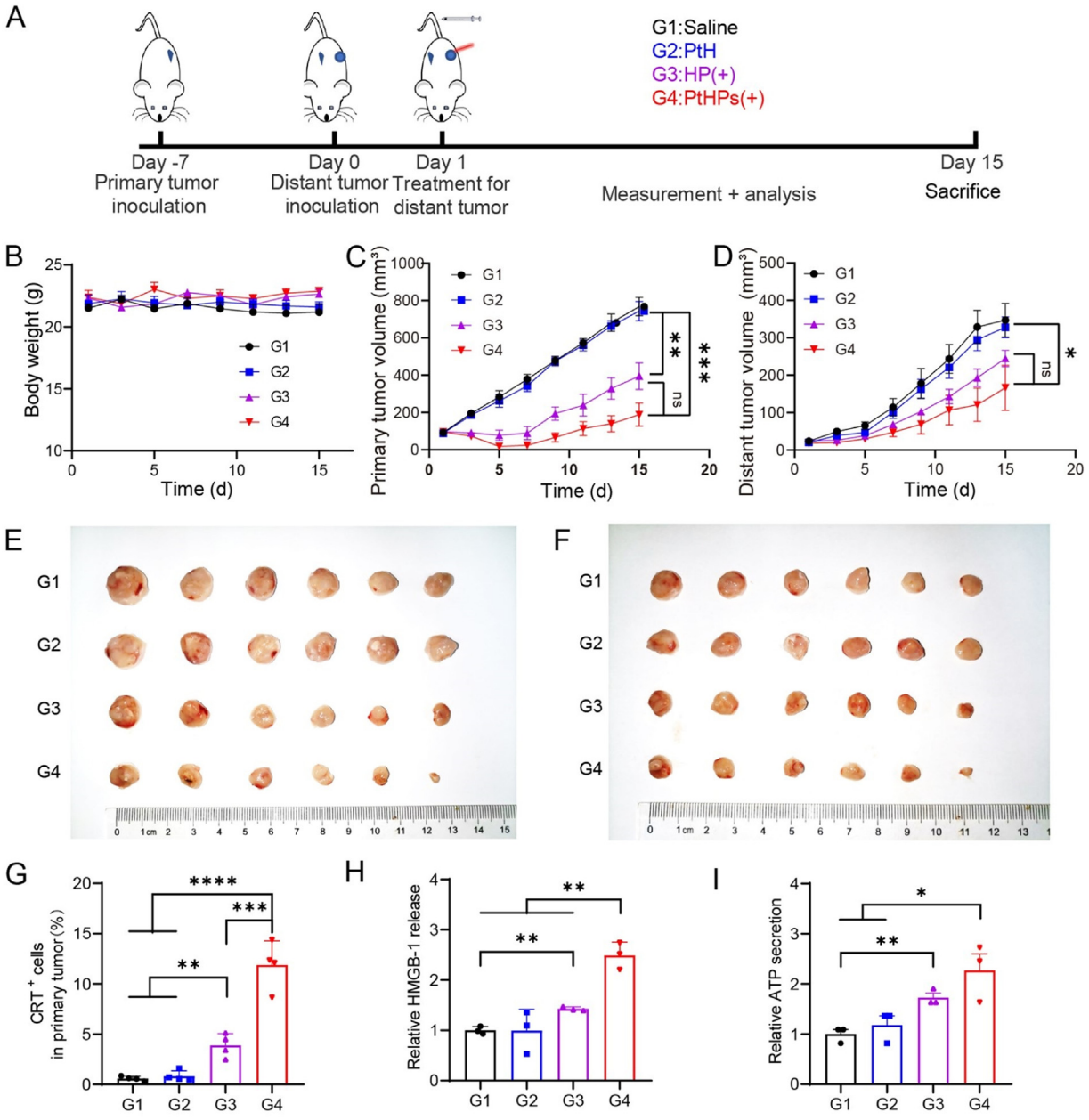

Fig. 6 – Antitumor effects of PtHPs in a bilateral tumor model. (A) Experimental design. (B) Body weight changes ($n = 6$). Tumor growth curves for (C) the primary tumors and (D) the distant tumors in each treatment group ($n = 6$). Images of (E) the primary tumors and (F) the distant tumors at the end of treatments. (G) Levels of CRT^+ cells in the primary tumors after treatment ($n = 4$). (H) HMGB-1 release in the primary tumors after treatment ($n = 3$). (I) ATP secretion in the primary tumors after treatment ($n = 3$). G1: saline, G2: PtH, G3: HP(+), G4: PtHPs(+). Data are expressed as mean ± SEM. *$P < 0.05$, **$P < 0.01$, ***$P < 0.001$.

group, respectively (Fig. 7G and 7H). The increased infiltration of CD3, CD4 and CD8 T cells in lymph nodes indicated the proliferation and differentiation of T cells (Figs. 7F, 7I and S23), which further illustrated the activation of antitumor immune responses. These results collectively show that PtHPs(+) treatment triggers strong and effective antitumor immune responses, as evidenced in the suppression of distant tumors (Fig. 6D and 6F). In addition, a significant increase in the proportion of effector memory T cells (T_{em}) and central memory T cells (T_{cm}) was observed in spleen (Figs. 7B, 7C and S24), implying that PtHPs(+) treatment not only triggers antitumor immune responses but also induces an immunological memory effect, which might suppress long-term tumor recurrence. In general, PtHPs(+) can induce powerful ICD, promote the body to produce immune response, induce the maturation of lymphocytes, and promote the invasion of T cells in tumors. It can also promote T_{em} and T_{cm} production.

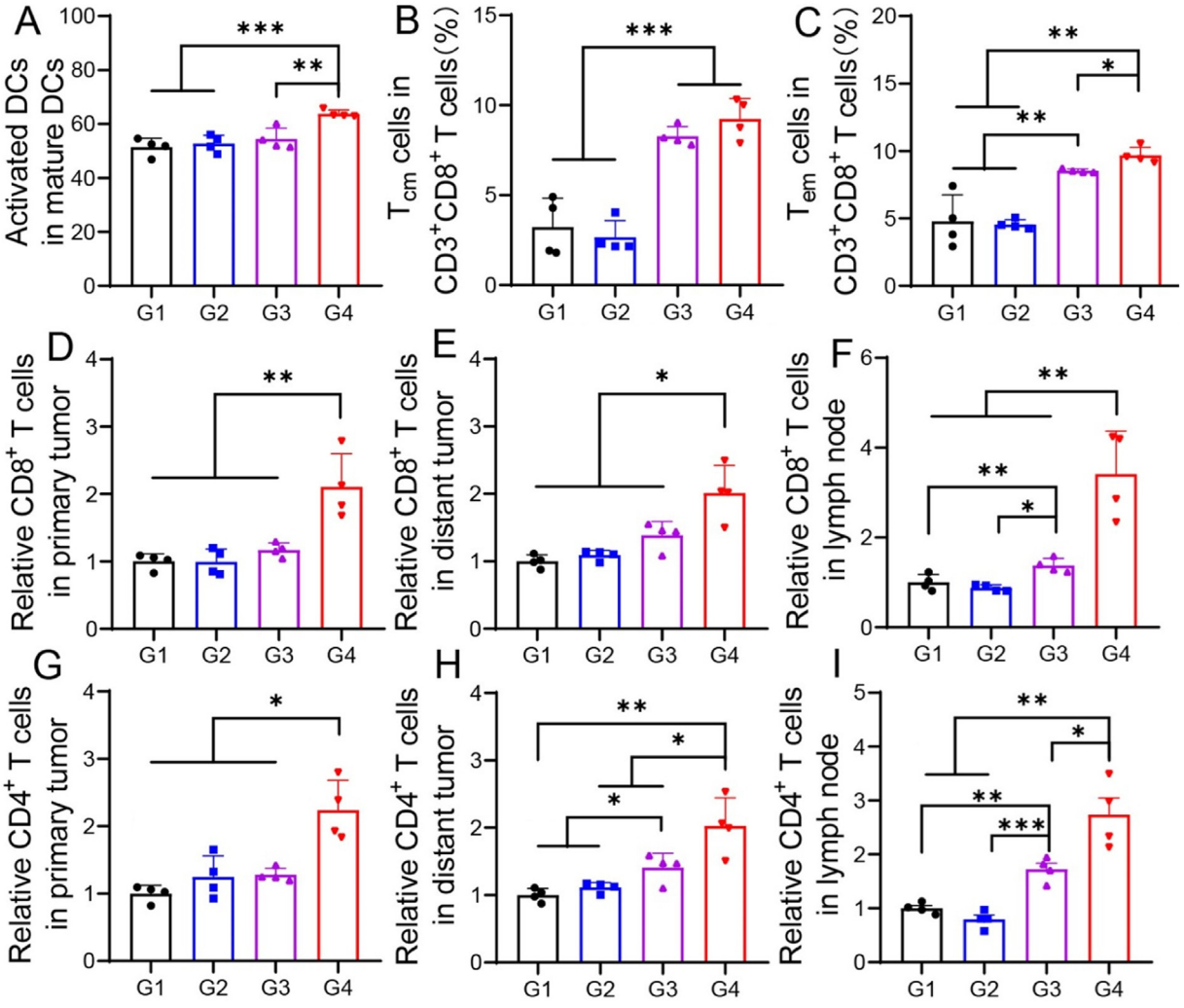

Fig. 7 – PtHPs-based PDT activates antitumor immune responses *in vivo*. Flow cytometric analyses of (A) $CD11c^+CD80^+$ $CD86^+$DCs, (B) central memory T cells, and (C), effective memory T cells in lymph nodes. Levels of (D) $CD8^+$ and (G) $CD4^+$ T cell infiltration in primary tumors after treatment. Levels of (E) $CD8^+$ and (H) $CD4^+$ T cell infiltration in distant tumors after treatment. Levels of (F) $CD8^+$ and (I) $CD4^+$ T cell infiltration in lymph nodes after treatment. G1: saline, G2: PtH, G3: HP(+), G4: PtHPs(+). Data are expressed as mean ± SEM. *$P < 0.05$, **$P < 0.01$, ***$P < 0.001$, ns stands for not significant.

4. Conclusion

In summary, we designed and prepared a new nanomedicine PtHPs by co-assembling two HES conjugates PtH and HP. PtHPs have good aqueous solubility, excellent photostability, long circulation capacity, high tumor targeting and enrichment efficiency, and decent biosafety. Within tumor cells, PtHPs generate ROS via illumination to trigger PDT. Meanwhile, Pt (IV) in PtHPs consumes GSH to release Pt (II), which further inhibits TrxR activity. Therefore, PtHPs boost the production of ROS by destroying intracellular antioxidant systems and overcome the problem that PDT is limited by high reduction force within tumor cells, amplifying oxidative stress and ICD effects. As a result, PtHPs(+) promotes DC cells maturation and induces T cell-mediated immune responses to suppress the growths of both primary and distal tumors.

This study solves the problem that photosensitizers have poor water solubility and cannot target tumor enrichment. In view of the problem that PDT is inhibited by the intracellular antioxidant system, it is proposed to achieve double inhibition by Pt (IV) to promote PDT and induce stronger immune response. Some studies have solved the problem of water solubility of photosensitizers by PEG modification and other methods [55,56]. Compared with these methods, HES we used has the advantages of good water solubility, biocompatibility, biodegradability and rich chemical modification groups. Some studies have solved the problem that PDT is inhibited by intracellular antioxidant system by adding antioxidant system inhibitors [22]. Compared with these methods, we used cisplatin-based Pt (IV), which has a certain chemotherapeutic effect while dually inhibiting the antioxidant system. Although PtHPs have a good antitumor effect, it can be further improved. The rich chemical

modification groups on HES can further modify the targeting groups and improve the targeting effect. Although there are some shortcomings, this study reports a new HES-based nanomedicine that provides a new paradigm for promoting PDT efficacy by inhibiting both the GSH system and the Trx system.

Conflicts of interest

The authors (Z. Li, X. Yang and X. Chen) have submitted patent applications associated with this research.

CRediT authorship contribution statement

Xiang Chen: Writing – original draft, Methodology, Investigation. **Zhengtao Yong:** Methodology, Investigation. **Yuxuan Xiong:** Methodology, Investigation. **Hai Yang:** Methodology, Investigation. **Chen Xu:** Methodology, Investigation. **Xing Wang:** Methodology, Investigation. **Qingyuan Deng:** Methodology, Investigation. **Jiayuan Li:** Methodology, Investigation. **Xiangliang Yang:** Supervision, Funding acquisition. **Zifu Li:** Writing – review & editing, Validation, Supervision, Project administration, Funding acquisition, Data curation, Conceptualization.

Acknowledgment

We thank the Research Core Facilities for Life Science (HUST), the Optical Bioimaging Core Facility of WNLO-HUST, and the Analytical and Testing Center of HUST for the facility support. This work was financially supported by grants from the National Research and Development Program of China (2020YFA0211200, 2020YFA0710700), the National Science Foundation of China (82172757), the Program for HUST Academic Frontier Youth Team (2018QYTD01), the HCP Program for HUST, and the Opening fund of Hubei Key Laboratory of Bioinorganic Chemistry & Materia Medica (No. BCMM202302).

Supplementary materials

Supplementary material associated with this article can be found, in the online version, at doi:10.1016/j.ajps.2024.100950.

References

[1] Wang NH, Zhao ZY, Xiao X, Mo L, Yao W, Yang HK, et al. ROS-responsive self-activatable photosensitizing agent for photodynamic-immunotherapy of cancer. Acta Biomater 2023;164:511–21.
[2] Ji XY, Ge LL, Liu C, Tang ZM, Xiao YF, Chen W, et al. Capturing functional two-dimensional nanosheets from sandwich-structure vermiculite for cancer theranostics. Nat Commun 2021;12:1124.
[3] Kang Y, Mao Z, Wang Y, Pan C, Ou MT, Zhang HJ, et al. Design of a two-dimensional interplanar heterojunction for catalytic cancer therapy. Nat Commun 2022;13:2425.
[4] Zhang HJ, Mao Z, Kang Y, Zhang W, Mei L, Ji XY. Redox regulation and its emerging roles in cancer treatment. Coordin Chem Rev 2023;475:214897.
[5] Xie JL, Wang YW, Choi W, Jangili P, Ge YQ, Xu Y, et al. Overcoming barriers in photodynamic therapy harnessing nano-formulation strategies. Chem Soc Rev 2021;50: 9152–9201.
[6] Li XS, Lovell JF, Yoon J, Chen XY. Clinical development and potential of photothermal and photodynamic therapies for cancer. Nat Rev Clin Oncol 2020;17:657–74.
[7] Vankayala R, Hwang KC. Near-infrared-light-activatable nanomaterial-mediated phototheranostic nanomedicines: an emerging paradigm for cancer treatment. Adv Mater 2018;30:1706320.
[8] Fan WP, Huang P, Chen XY. Overcoming the Achilles' heel of photodynamic therapy. Chem Soc Rev 2016;45:6488–519.
[9] Zhou ZJ, Song JB, Nie LM, Chen XY. Reactive oxygen species generating systems meeting challenges of photodynamic cancer therapy. Chem Soc Rev 2016;45:6597–626.
[10] Choi J, Sun IC, Hwang HS, Yoon HY, Kim K. Light-triggered photodynamic nanomedicines for overcoming localized therapeutic efficacy in cancer treatment. Adv Drug Deliver Rev 2022;186:114344.
[11] Zhang SW, Wang J, Kong ZQ, Sun XX, He ZG, Sun BJ, et al. Emerging photodynamic nanotherapeutics for inducing immunogenic cell death and potentiating cancer immunotherapy. Biomaterials 2022;282:121433.
[12] Li W, Yang J, Luo LH, Jiang MS, Qin B, Yin H, et al. Targeting photodynamic and photothermal therapy to the endoplasmic reticulum enhances immunogenic cancer cell death. Nat Commun 2019;10:3349.
[13] Gao J, Wang WQ, Pei Q, Lord MS, Yu HJ. Engineering nanomedicines through boosting immunogenic cell death for improved cancer immunotherapy. Acta Pharmacol Sin 2020;41:986–94.
[14] Agostinis P, Berg K, Cengel KA, Foster TH, Girotti AW, Gollnick SO, et al. Photodynamic therapy of cancer: an update. Ca-Cancer. J Clin 2011;61:250–81.
[15] Duan XP, Chan C, Lin WB. Nanoparticle-mediated immunogenic cell death enables and potentiates cancer immunotherapy. Angew Chem Int Edit 2019;58:670–80.
[16] Radogna F, Diederich M. Stress-induced cellular responses in immunogenic cell death: implications for cancer immunotherapy. Biochem Pharmacol 2018;153:12–23.
[17] Gong T, Liu L, Jiang W, Zhou RB. DAMP-sensing receptors in sterile inflammation and inflammatory diseases. Nat Rev Immunol 2020;20:95–112.
[18] Ahmed A, Tait SWG. Targeting immunogenic cell death in cancer. Mol Oncol 2020;14:2994–3006.
[19] Li ZL, Lai XQ, Fu SQ, Ren L, Cai H, Zhang H, et al. Immunogenic Cell Death activates the tumor immune microenvironment to boost the immunotherapy efficiency. Adv Sci 2022;9:2201734.
[20] Jung E, Kwon S, Song N, Kim N, Jo H, Yang M, et al. Tumor-targeted redox-regulating and antiangiogenic phototherapeutics nanoassemblies for self-boosting phototherapy. Biomaterials 2023;298:122127.
[21] Li YS, He G, Fu LH, Younis MR, He T, Chen YZ, et al. A microneedle patch with self-oxygenation and glutathione depletion for repeatable photodynamic therapy. ACS Nano 2022;16:17298–312.
[22] Zhang HY, Kong ZQ, Wang ZY, Chen Y, Zhang SW, Luo C. Molecularly engineering a dual-drug nanoassembly for self-sensitized photodynamic therapy via thioredoxin impairment and glutathione depletion. Drug Deliv 2022;29:3281–90.
[23] Chen W, He H, Jiao P, Han L, Li J, Wang X, et al. Metal-organic framework for hypoxia/ROS/pH triple-responsive cargo release. Adv Healthc Mater 2023;12:2301785.

[24] Du J, Wei Y, Zhao Y, Xu F, Wang Y, Zheng W, et al. A photoactive platinum(IV) anticancer complex inhibits thioredoxin-thioredoxin reductase system activity by induced oxidization of the protein. Inorg Chem 2018;57:5575–84.
[25] Prast-Nielsen S, Cebula M, Pader I, Arner ES. Noble metal targeting of thioredoxin reductase–covalent complexes with thioredoxin and thioredoxin-related protein of 14 kDa triggered by cisplatin. Free Radic Biol Med 2010;49:1765–78.
[26] Witte AB, Anestal K, Jerremalm E, Ehrsson H, Arner ES. Inhibition of thioredoxin reductase but not of glutathione reductase by the major classes of alkylating and platinum-containing anticancer compounds. Free Radic Biol Med 2005;39:696–703.
[27] Lu HT, He SS, Zhang QF, Li XY, Xie ZG, Wang ZG, et al. Dual-sensitive dual-prodrug nanoparticles with light-controlled endo/lysosomal escape for synergistic photoactivated chemotherapy. Biomater Sci-Uk 2021;9:7115–23.
[28] Rottenberg S, Disler C, Perego P. The rediscovery of platinum-based cancer therapy. Nat Rev Cancer 2021;21:37–50.
[29] Qi LY, Luo Q, Zhang YY, Jia FF, Zhao Y, Wang FY. Advances in toxicological research of the anticancer drug cisplatin. Chem Res Toxicol 2019;32:1469–86.
[30] Moynihan E, Panseri S, Bassi G, Rossi A, Campodoni E, Dempsey E, et al. Development of novel Pt(IV)-carbohydrate derivatives as targeted anticancer agents against osteosarcoma. Int J Mol Sci 2023;24:6028.
[31] Huang H, Dong Y, Zhang YH, Ru D, Wu ZH, Zhang JL, et al. GSH-sensitive Pt(IV) prodrug-loaded phase-transitional nanoparticles with a hybrid lipid-polymer shell for precise theranostics against ovarian cancer. Theranostics 2019;9:1047–65.
[32] Aher S, Zhu J, Bhagat P, Borse L, Liu X. Pt(IV) complexes in the search for novel platinum prodrugs with promising activity. Top Curr Chem (Cham) 2024;382:6.
[33] Zhao ZH, Wang WQ, Li CX, Zhang YQ, Yu TR, Wu RF, et al. Reactive oxygen species-activatable liposomes regulating hypoxic tumor microenvironment for synergistic photo/chemodynamic therapies. Adv Funct Mater 2019;29:1905013.
[34] Wang B, Zhou J, Li R, Tang D, Cao Z, Xu C, et al. Activating CD8(+) T cells by Pt(IV) prodrug-based nanomedicine and aPD-L1 antibody for enhanced cancer immunotherapy. Adv Mater 2024;36(21):2311640.
[35] Johnstone TC, Suntharalingam K, Lippard SJ. The next generation of platinum drugs: targeted Pt(II) agents, nanoparticle delivery, and Pt(IV) prodrugs. Chem Rev 2016;116:3436–86.
[36] Zajac J, Novohradsky V, Markova L, Brabec V, Kasparkova J. Platinum (IV) derivatives with cinnamate axial ligands as potent agents against both differentiated and tumorigenic cancer stem rhabdomyosarcoma cells. Angew Chem Int Edit 2020;59:3329–35.
[37] Zheng S, Li G, Shi J, Liu X, Li M, He Z, et al. Emerging platinum(IV) prodrug nanotherapeutics: a new epoch for platinum-based cancer therapy. J Control Release 2023;361:819–46.
[38] Deng Z, Zhu G. Beyond mere DNA damage: recent progress in platinum(IV) anticancer complexes containing multi-functional axial ligands. Curr Opin Chem Biol 2023;74:102303.
[39] Xiong YX, Yong ZT, Li SY, Wang Q, Chen X, Zhang ZJ, et al. Self-reliant nanomedicine with long-lasting glutathione depletion ability disrupts adaptive redox homeostasis and suppresses cancer stem cells. Adv Funct Mater 2023;34(8):2310158.
[40] Xiao C, Li JY, Wang X, Li SY, Xu C, Zhang ZJ, et al. Hydroxyethyl starch stabilized copper-diethyldithiocarbamate nanocrystals for cancer therapy. J Controll Rel 2023;356:288–305.
[41] Chen JT, Li S, Liu X, Liu S, Xiao C, Zhang ZJ, et al. Transforming growth factor-β blockade modulates tumor mechanical microenvironments for enhanced antitumor efficacy of photodynamic therapy. Nanoscale 2021;13.
[42] Wang C, Wang HM, Yang H, Xu C, Wang Q, Li Z, et al. Targeting cancer-associated fibroblasts with hydroxyethyl starch nanomedicine boosts cancer therapy. Nano Res 2023;16:7323–36.
[43] Xiao C, Hu H, Yang H, Li S, Zhou H, Ruan J, et al. Colloidal hydroxyethyl starch for tumor-targeted platinum delivery. Nanoscale Adv 2019;1:1002–12.
[44] Fang ZX, Lin L, Li ZQ, Gua L, Pan DY, Li YK, et al. Stimuli-responsive heparin-drug conjugates co-assembled into stable nanomedicines for cancer therapy. Acta Biomater 2023;164:422–34.
[45] Zhang XQ, Wu YH, Li ZQ, Wang WJ, Wu YP, Pan DY, et al. Glycodendron/pyropheophorbide-a (Ppa)-functionalized hyaluronic acid as a nanosystem for tumor photodynamic therapy. Carbohyd Polym 2020;247:116749.
[46] Sun BJ, Chen Y, Yu H, Wang C, Zhang XB, Zhao HQ, et al. Photodynamic PEG-coated ROS-sensitive prodrug nanoassemblies for core-shell synergistic chemo-photodynamic therapy. Acta Biomater 2019;92:219–28.
[47] Wang C, Wang Q, Wang HM, Li Z, Chen JT, Zhang ZJ, et al. Hydroxyethyl starch-folic acid conjugates stabilized theranostic nanoparticles for cancer therapy. J Controll Rel 2023;353:391–410.
[48] Hu H, Li Y, Zhou Q, Ao Y, Yu C, Wan Y, et al. Redox-sensitive hydroxyethyl starch-doxorubicin conjugate for tumor targeted drug delivery. ACS Appl Mater Interfaces 2016;8:30833–44.
[49] Wan Q Zhang RY, Zhuang ZY, Li YX, Wang ZM, Zhang WJ, et al. Molecular engineering to boost AIE-active free radical photogenerators and enable high-performance photodynamic therapy under hypoxia. Adv Funct Mater 2024;34:2312870.
[50] Wen KK Wu LF, Wu XX, Lu Y, Duan T, Ma H, et al. Precisely tuning photothermal and photodynamic effects of polymeric nanoparticles by controlled copolymerization. Angew Chem Int Edit 2020;59:12756.
[51] Donahue ND, Acar H, Wilhelm S. Concepts of nanoparticle cellular uptake, intracellular trafficking, and kinetics in nanomedicine. Adv Drug Deliver Rev 2019;143:68.
[52] Han XBB, Li HXX, Jiang YQQ, Wang H, Li XSS, Kou JYY, et al. Upconversion nanoparticle-mediated photodynamic therapy induces autophagy and cholesterol efflux of macrophage-derived foam cells via ROS generation. Cell Death Dis 2017;8:e2864.
[53] Zeng YP, Li SF, Zhang SF, Wang L, Yuan H, Hu FQ. Cell membrane coated-nanoparticles for cancer immunotherapy. Acta Pharm Sin B 2022;12:3233–54.
[54] Huang PY, Liang SY, Xiang Y, Li MR, Wang MR, Liu LH. Endoplasmic reticulum-targeting self-assembly nanosheets promote autophagy and regulate immunosuppressive tumor microenvironment for efficient photodynamic immunotherapy. Small 2024;20(25):2311056.
[55] Wang S, Yu GC, Yang WJ, Wang ZT, Jacobson O, Tian R, et al. Photodynamic-chemodynamic Cascade reactions for efficient drug delivery and enhanced combination therapy. Adv Sci 2021;8:2002927.
[56] Zheng XL, Pan DY, Chen XT, Wu L, Chen M, Wang WJ, et al. Self-stabilized supramolecular assemblies constructed from PEGylated dendritic peptide conjugate for augmenting tumor retention and therapy. Adv Sci 2021;8:2102741.